Journal of South American Earth Sciences 35 (2012) 62–73

Contents lists available at SciVerse ScienceDirect

Journal of South American Earth Sciences

journal homepage: www.elsevier.com/locate/jsames

# Mineralogical, IR-spectral and geochemical monitoring of hydrothermal alteration in a deformed and metamorphosed Jurassic VMS deposit at Arroyo Rojo, Tierra del Fuego, Argentina

C. Biel [a,b], I. Subías [a,*], R.D. Acevedo [c], I. Yusta [d], F. Velasco [d]

[a] Grupo Recursos Minerales, Universidad de Zaragoza, Pedro Cerbuna, 12, 50009 Zaragoza, Spain
[b] PROMINDSA (Productos Minerales para la Industria, S.A.), Zaragoza, Spain
[c] Centro Austral de Investigaciones Científicas (CADIC), Ushuaia, Argentina
[d] Dpto. Mineralogía-Petrología, Universidad del País Vasco-UPV/EHU, Spain

ARTICLE INFO

*Article history:*
Received 10 February 2011
Accepted 21 November 2011

*Keywords:*
Fuegian Andes
VMS
Hydrothermal alteration
Mineral chemistry
PIMA

ABSTRACT

The Arroyo Rojo Zn–Pb–Cu volcanogenic massive sulfide deposit is the main deposit of the Fin del Mundo District in the Fuegian Andes, Argentina. This deposit is hosted by a Middle Jurassic volcanic and volcanoclastic sequence forming the Lemaire Formation. The latter consists, from the base up, of the following: rhyolitic and dacitic porphyritic rocks, ignimbrite, tuff, and flow. It is underlain by a pre-Jurassic basement and overlain by the hyaloclastic andesites of the Yahgán Formation. The Arroyo Rojo consists of stacked lenticular lenses that are associated with disseminated mineralization in both the footwall and the hanging wall. The internal structure of the ore lenses is marked by the occurrence of massive, semi-massive and banded facies, along with stringer and brecciated zones and minor ore disseminations. The mineral assemblage comprises mainly pyrite and sphalerite, with minor amounts of galena and chalcopyrite and rare pyrrhotite, arsenopyrite, tetrahedrite and bournonite. The ores and the volcanic host rocks have metamorphosed to greenschist facies and were overprinted by a penetrative tectonic foliation, which led to the development of mylonitic, and cataclastic textures, recrystallization and remobilization.

Primary depositional characteristics and regional and hydrothermal alteration patterns were preserved despite deformation and metamorphism. Therefore, primary banding was preserved between facies boundaries. In addition, some remnants of magmatic origin are recognizable in preserved phenocrysts and volcaniclastic phenoclasts. Most of the volcanic and volcaniclastic rocks of the host sequence show a rhyolitic to rhyo-dacitic composition.

Regional seafloor alteration, characterized by the presence of clinozoisite, Fe-chlorite and titanite, along with quartz and albite, is partially obliterated by hydrothermal alteration. The hydrothermal alteration is stratabound with the following assemblages, which developed from the base to top: (1) Quartz-Chlorite ± Sericite, (2) Quartz-Chlorite, (3) Chlorite ± Quartz-Sericite-Calcite, (4) Quartz-Chlorite ± Calcite and (5) Sericite + Quartz ± Chlorite ± Calcite. Magnesium-chlorite and phengitic white mica typically occur in the vicinity of the Arroyo Rojo ore lenses. To provide field criteria for exploration vectoring, the chemical composition of chlorite and the phengitic and paragonitic content of the white mica were determined and correlated with PIMA Fe–OH and Al–OH absorption wavelengths, respectively, relative to their proximity to the mineralized lenses.

The results of this study can be used to help identify (1) felsic proximal facies associations, (2) ore horizons and (3) favorable hydrothermal alteration zones in other parts of the Fin del Mundo district.



## 1. Introduction

The Arroyo Rojo deposit is a polymetallic Zn–Pb–Cu–Ag volcanic-hosted massive sulfide (VMS) deposit that consists of stacked lenses hosted in Jurassic rhyolitic volcanic rocks that form a linear belt in the Andes of Tierra del Fuego (Ametrano et al., 2000;

* Corresponding author. Fax: +34 976 761 106.
*E-mail address:* isubias@unizar.es (I. Subías).

0895-9811/$ – see front matter © 2011 Elsevier Ltd. All rights reserved.
doi:10.1016/j.jsames.2011.11.005

Broili et al., 2000; Biel et al., 2010) (Fig. 1). Exploration conducted by several companies has outlined two main targets: Sierra de Sorondo and Sierra de Alvear, two parallel E–W trending mountain ranges belonging to the Fuegian Andes (Fig. 1). Polymetallic sulfide occurs as disseminations, stringers, and semi-massive to massive lenses, outcropping widely along these two ranges. The area as a whole is now referred to as the Fin del Mundo mining district (Broili et al., 2000). Despite significant exploration, sufficient field criteria have yet to be developed to provide a vector toward potential ore zones. With this in mind, the current study was undertaken to characterize the lithogeochemical and mineralogical alteration halo surrounding the Arroyo Rojo, which represents the major deposit in the study area.

The absence of well-defined mineral alteration zones as a result of the development of intense foliation and mylonitization has hindered field identification and hydrothermal alteration mapping. Nevertheless, the use of a Portable Mineral Analyzer (PIMA) using an SWIR spectral range (Short Wave Infrared: 1300–2500 nm) has proved a powerful tool in this context. As demonstrated here, this technique is able to distinguish between minor compositional variations in hydrous minerals (e.g., chlorite and white mica).

The aim of this paper is to document the type of hydrothermal alteration of the Arroyo Rojo VMS deposit, and determine the spatial distribution of the main alteration minerals recognized by PIMA spectral analysis. The integration of all these data allows us to develop a hydrothermal alteration model for the deposit and to define prospecting criteria applicable to other zones of the volcanic belt of Tierra de Fuego.

## 2. Regional geology

The study area is located on the Isla Grande de Tierra del Fuego (Fig. 1), which is the largest of the Fuegian Archipelago islands, located in southern Argentina between latitude 53–56°S and longitude 66–72°W. The Isla Grande is situated at the boundary between the South America and Scotia tectonic plates, which are separated by the Magellan Fault. The VMS deposits of the Fin del Mundo district occur on the Scotia Plate whose geology is related to the succession of extensive to compressive and transcurrent tectonic regimes related to three major orogenic cycles: the Gondwanian, Patagonian, and Andean cycles. Triassic rifts related to the breakup of Gondwana were reactivated in Early to Middle Jurassic times, generating a back-arc basin at Gondwana's margin. Felsic volcanism associated with this event is intercalated with multiple marine deposition episodes. The resulting volcanic, volcanoclastic, and pelagic marine sequence comprise the Lemaire Formation.

Jurassic rifting evolved into a back-arc basin, contemporary to the basic volcanism that produced the oceanic crust (Dalziel et al., 1974). Abundant outcrops of Late Jurassic to Early Cretaceous basic pillow lavas (Ophiolitic Tortuga Complex and Sarmiento Formation) represent remnants of this oceanic floor. Synchronously, marine

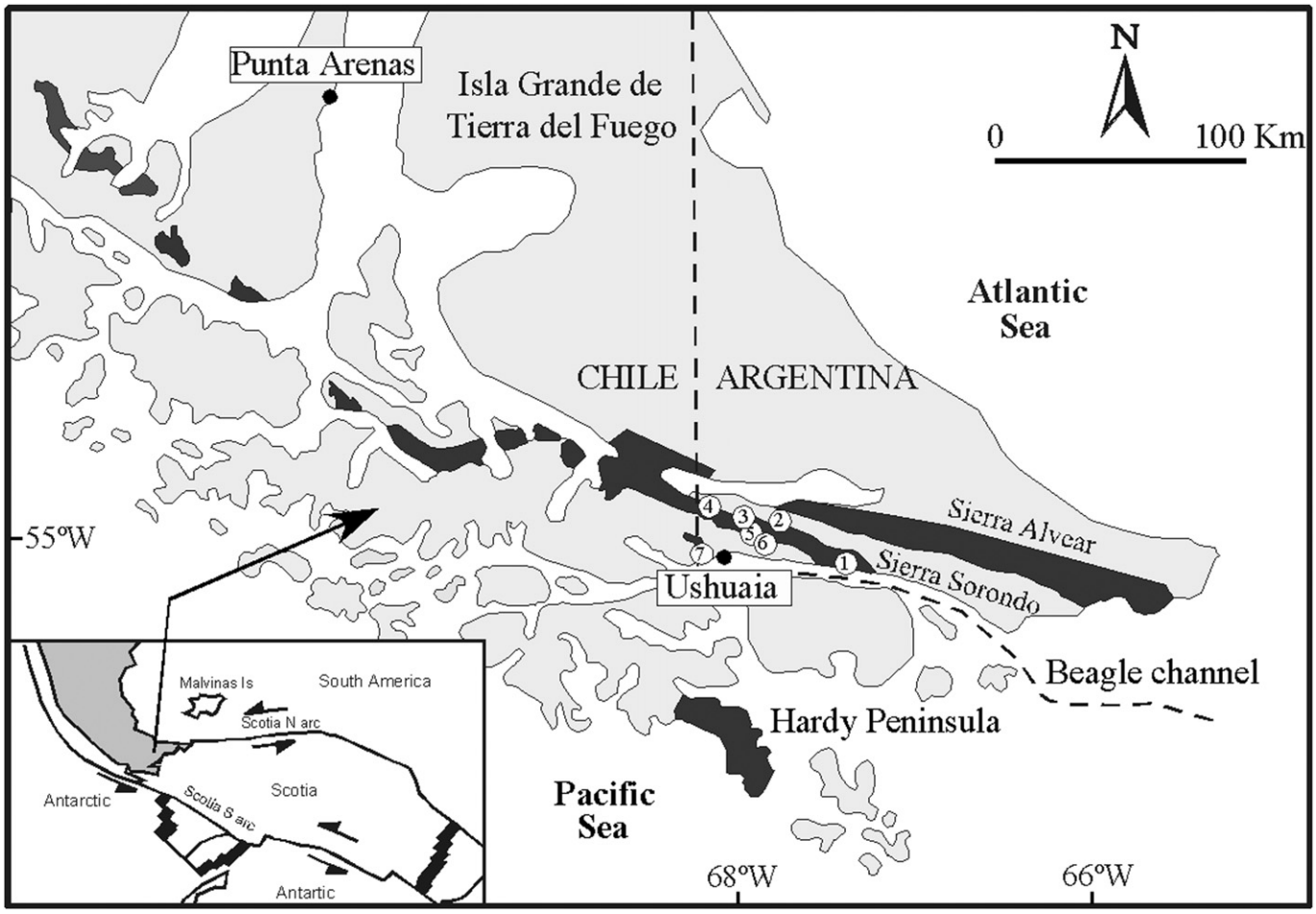


**Fig. 1.** Rhyolitic belt of the Andes Fueguinos, showing the location of the volcanic-hosted massive sulfide prospects (1: Puerto Almansa; 2: Gregores; 3: Sargent; 4: Rancho Hambre; 5: Lago Guanaco; 6: Arroyo Rojo; 7: Beatriz mine). Inset is a plate tectonic map of Tierra del Fuego (Barker, 2001).

sedimentation in the basin gave rise to the Springhill Formation in proximal areas and to the Yahgán Formation in distal ones.

## 3. Geology of the Arroyo Rojo deposit

The Arroyo Rojo deposit occurs in a region with east–northeast-verging thrusts and folds within a Late Jurassic regional volcano-sedimentary complex (Lemaire Formation) and in proximity to the overlying turbidites of the Yahgán Formation. The deposit is stratigraphically underlain by rhyolites and dacites and overlain by a complex unit composed of felsic tuffs, ignimbrites, and flows (Fig. 2A). The regional metamorphic grade reached in the aforementioned Lemaire and Yahgán Formations is greenschist facies based on mineral assemblages and crystallochemical parameters of phyllosilicates (Olivero and Martinioni, 2001; Biel et al., 2007). Shear zones related to regional metamorphism are associated with the presence of penetrative structural fabrics and mylonitic foliation; as a consequence, both mylonites and metarhyolites have developed (Biel et al., 2010). Despite intense deformation and metamorphism, protoliths are still recognizable.

At the Arroyo Rojo deposit, massive sulfide lenses have developed at several stratigraphic levels and are connected by an alteration zone that contains disseminated sulfides (Fig. 2B) or a zone of veins parallel to or cutting the foliation at a low angle. Despite their short lengths, these veins are limited to the footwall in what seems to preclude a remobilization process linked to deformation. Therefore, we consider them stringers. Surface and drilling programs indicated interceptions between 1.5 and 4 m thick with a true thickness at depths between 3 and 18.6 m of 1% Cu, 1.4% Pb, and 3% Zn. The stockwork zone has not been found in either the surface exposures or the investigated drill holes. The ore body has a pyrite-rich base that passes upward through a massive ore to a laminated upper portion. Ore minerals include pyrite, sphalerite, chalcopyrite, galena, and minor tetrahedrite and bournonite. Barite,

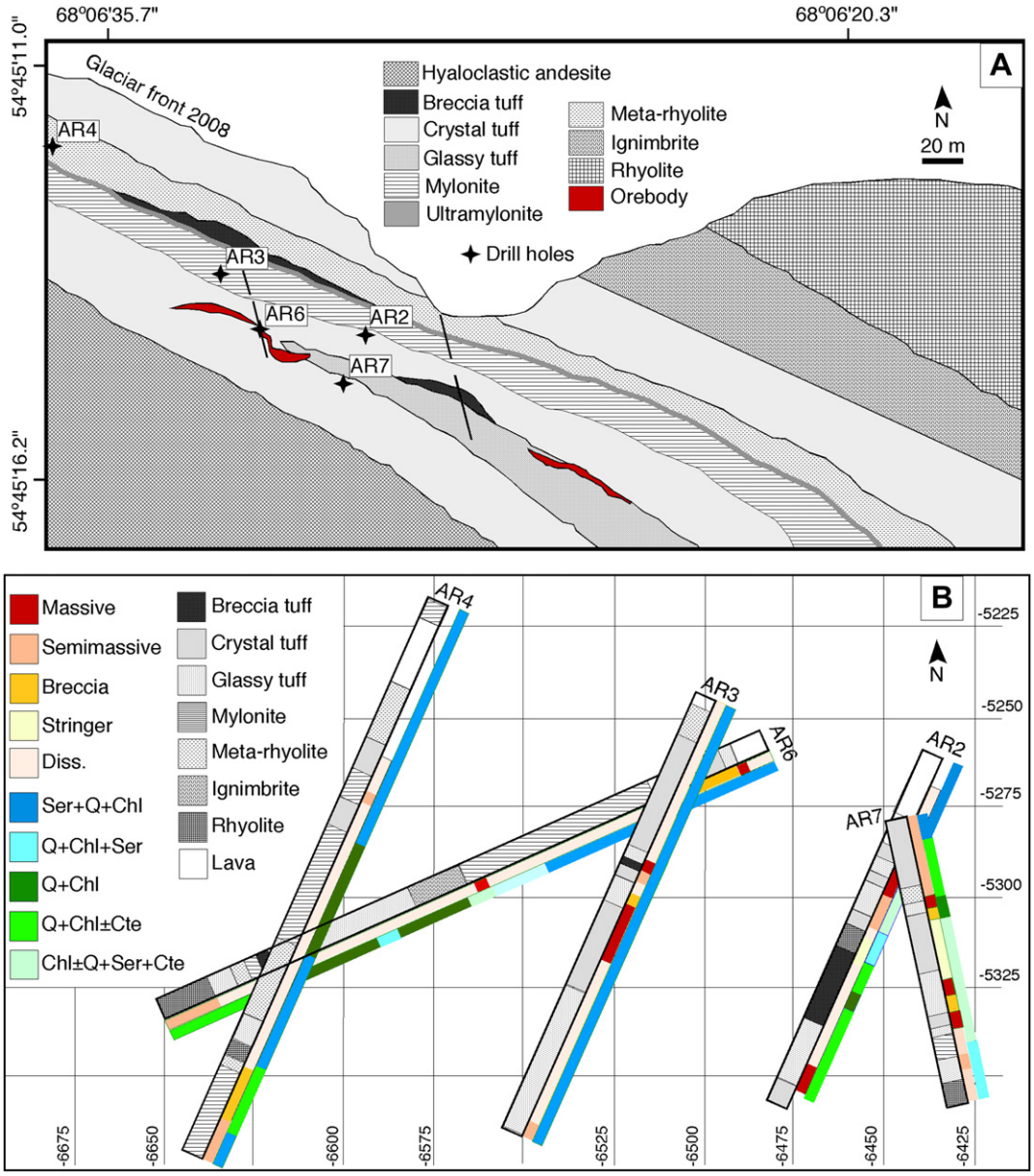


**Fig. 2.** A) Geological map of the Arroyo Rojo deposit showing the location of drill holes and volcanic sequence. Massive sulfide lenses are drawn in red. B) Drill core sketch map showing the relation between mineralization, alteration, and lithotypes. Q: Quartz; Chl: Chlorite; Ser: Sericite; Cte: Calcite; Diss.: Disseminated ores. (For interpretation of the references to color in this figure legend, the reader is referred to the web version of this article.)

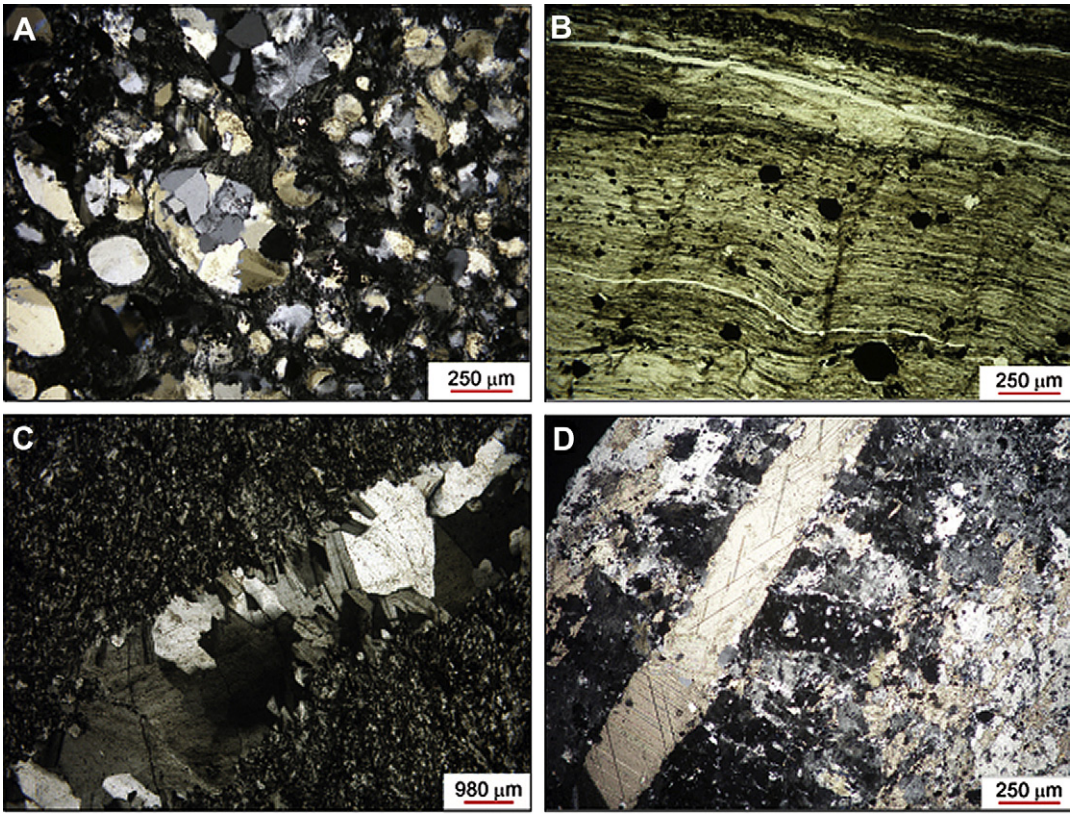


**Fig. 3.** Photomicrographs of A) devitrified glass vesicles totally replaced by mono- and polycrystalline quartz under crossed polars; B) chloritite with pyrite disseminations under parallel polars; C) open space adularia filling in an albitized rock under crossed polars; D) quartz and calcite association in a mineralized rock also showing spar calcite as fracture fillings under crossed polars.

Fe oxides, and chert are not present within or above the massive sulfide lenses.

## 4. Samples and methods

A suite of over 160 samples from 5 drill cores (AR2, AR3, AR4, AR6, and AR7) and 50 samples from surface exposures covering all lithological units, mineralizations and alteration styles recognized in the deposit were collected. In addition, 10 samples of weakly altered or unaltered host rocks belonging to the Lemaire Formation were gathered for comparison purposes in areas with no mineralization and/or without hydrothermal alteration. The latter samples will be referred to in this paper as regional rocks.

Mineral identification has been performed by means of optical and scanning electron microscopy (SEM), X-ray Diffraction (XRD), Portable Mineral Analyzer (PIMA) and electron microprobe (EPMA).

After grinding and homogenizing the selected samples to powders of $<53$ μm in grain size, their global mineralogy was studied with XRD. Oriented aggregates (OA) were prepared by both the $<20$ μm fractions separated by sedimentation. The XRD data were processed with the XPowder software (Martin, 2004).

White mica and chlorite composition were determined by a Cameca SX-50 electron microprobe at the Universidad de Barcelona. Structural formulae of the aforementioned phyllosilicates were calculated based on 22 and 28 oxygens, respectively.

Special sample preparation is not necessary for the PIMA SP Infrared Spectrometer because data acquisition is performed by placing a clean, flat and dry sample surface on the spectrometer window (10 mm). Infrared spectra were stored as computer files with the Pimaview 3.1 software. This software allows us to

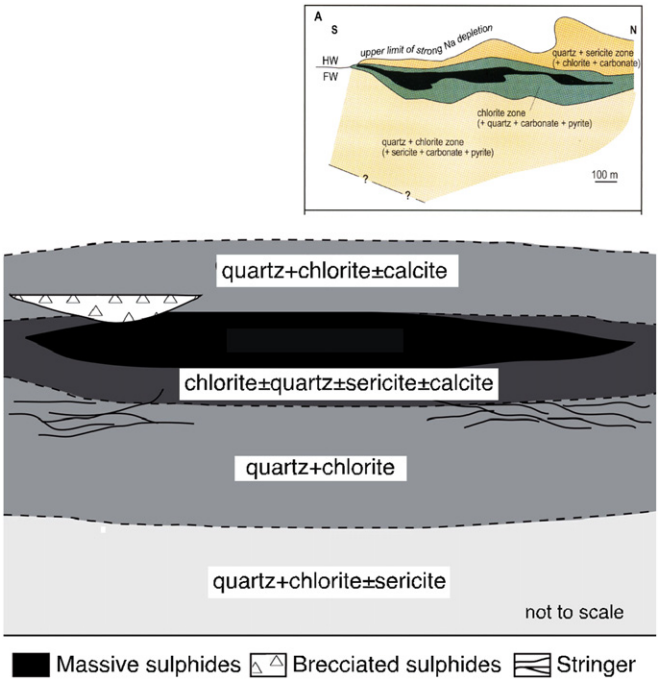


**Fig. 4.** Schematic diagram showing the distribution of hydrothermal alteration zones related to the Arroyo Rojo deposit. An example of stratabound altered zones (Gifkins et al., 2005) is included for comparison purposes. Cp: chalcopyrite; Po: pyrrhotite, Py: pyrite; Sl: sphalerite; Td: tetrahedrite.

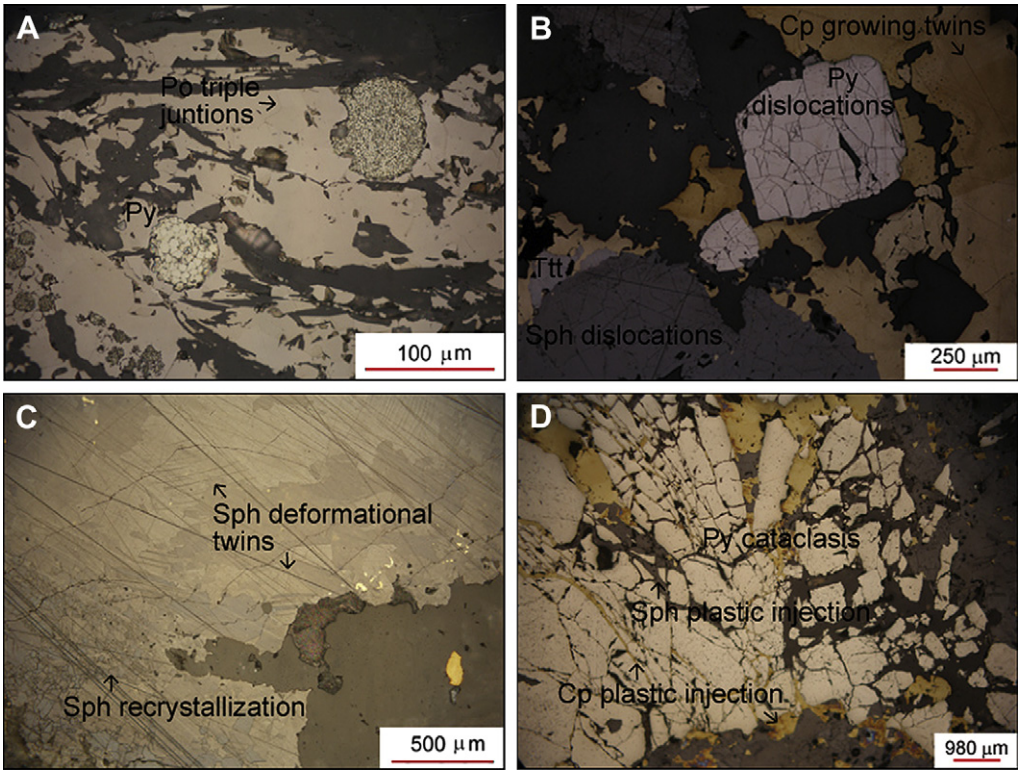


**Fig. 5.** Photomicrographs under parallel polars of A) polyframboids consisting of individual euhedral crystals; B) oriented planar dislocations in euhedral pyrite crystal; C) coarse sphalerite grains with deformational twins and fine-grained recrystallization on the rims; D) oriented fractures in pyrite with incipient developing of cataclastic flow.

**Table 1**
Selected electron probe microanalyses of white micas in the massive sulfide lenses and the related hydrothermal alteration of the Arroyo Rojo deposit (normalized to 22 oxygens $O_{10}(OH)_2$).

| | Distal ($n = 50$) | | | | Proximal ($n = 50$) | | | | Massive sulfide ($n = 4$) | | | |
|---|---|---|---|---|---|---|---|---|---|---|---|---|
| | Min | Max | Med | S.D | Min | Max | Med | S.D | Min | Max | Med | S.D |
| *wt %* | | | | | | | | | | | | |
| $SiO_2$ | 46.06 | 59.16 | 50.31 | 2.70 | 47.19 | 58.95 | 50.46 | 2.07 | 48.50 | 51.20 | 50.04 | 1.14 |
| $TiO_2$ | 0.00 | 2.50 | 0.14 | 0.40 | 0.00 | 0.19 | 0.06 | 0.04 | 0.02 | 0.04 | 0.03 | 0.01 |
| $Al_2O_3$ | 20.96 | 39.25 | 30.57 | 3.89 | 22.72 | 30.94 | 28.80 | 1.66 | 27.03 | 28.14 | 27.53 | 0.49 |
| FeO | 0.08 | 2.66 | 0.49 | 0.41 | 0.19 | 2.00 | 0.63 | 0.35 | 0.22 | 0.53 | 0.32 | 0.14 |
| MnO | 0.00 | 0.08 | 0.02 | 0.03 | 0.00 | 0.09 | 0.02 | 0.02 | 0.00 | 0.05 | 0.02 | 0.02 |
| MgO | 0.26 | 5.02 | 2.91 | 1.45 | 2.87 | 6.02 | 3.91 | 0.97 | 3.99 | 6.07 | 5.01 | 0.88 |
| CaO | 0.00 | 1.83 | 0.16 | 0.35 | 0.00 | 0.12 | 0.03 | 0.03 | 0.00 | 0.01 | 0.00 | 0.01 |
| $Na_2O$ | 0.00 | 5.34 | 0.88 | 1.56 | 0.00 | 0.35 | 0.12 | 0.07 | 0.06 | 0.09 | 0.07 | 0.02 |
| $K_2O$ | 2.28 | 10.60 | 8.63 | 2.44 | 8.72 | 10.96 | 10.34 | 0.51 | 10.23 | 11.05 | 10.75 | 0.36 |
| BaO | 0.00 | 1.10 | 0.40 | 0.30 | 0.00 | 0.77 | 0.36 | 0.20 | 0.00 | 0.63 | 0.36 | 0.26 |
| $H_2O$ | 4.14 | 4.83 | 4.44 | 0.15 | 4.30 | 4.72 | 4.49 | 0.07 | 4.31 | 4.54 | 4.46 | 0.10 |
| Total | 95.29 | 103.1 | 99.09 | 1.66 | 95.18 | 102.4 | 99.22 | 1.40 | 95.12 | 100.4 | 98.61 | 2.37 |
| *a.p.f.u.* | | | | | | | | | | | | |
| Si | 3.01 | 3.97 | 3.33 | 0.17 | 3.26 | 3.75 | 3.36 | 0.09 | 3.34 | 3.38 | 3.36 | 0.02 |
| Ti | 0.00 | 0.13 | 0.01 | 0.02 | 0.00 | 0.01 | 0.00 | 0.00 | 0.00 | 0.00 | 0.00 | 0.00 |
| Al IV | 0.03 | 0.99 | 0.67 | 0.17 | 0.25 | 0.74 | 0.64 | 0.09 | 0.62 | 0.66 | 0.64 | 0.02 |
| Al VI | 1.41 | 1.99 | 1.71 | 0.14 | 1.45 | 1.70 | 1.62 | 0.07 | 1.47 | 1.61 | 1.55 | 0.06 |
| Fe | 0.00 | 0.15 | 0.03 | 0.02 | 0.01 | 0.11 | 0.04 | 0.02 | 0.01 | 0.03 | 0.02 | 0.01 |
| Mn | 0.00 | 0.00 | 0.00 | 0.00 | 0.00 | 0.01 | 0.00 | 0.00 | 0.00 | 0.00 | 0.00 | 0.00 |
| Mg | 0.03 | 0.49 | 0.29 | 0.14 | 0.29 | 0.61 | 0.39 | 0.10 | 0.41 | 0.61 | 0.50 | 0.08 |
| Ca | 0.00 | 0.13 | 0.01 | 0.02 | 0.00 | 0.01 | 0.00 | 0.00 | 0.00 | 0.00 | 0.00 | 0.00 |
| Na | 0.00 | 0.67 | 0.11 | 0.19 | 0.00 | 0.05 | 0.02 | 0.01 | 0.01 | 0.01 | 0.01 | 0.00 |
| K | 0.19 | 0.89 | 0.73 | 0.21 | 0.73 | 0.93 | 0.88 | 0.05 | 0.91 | 0.94 | 0.92 | 0.01 |
| Ba | 0.00 | 0.03 | 0.01 | 0.01 | 0.00 | 0.02 | 0.01 | 0.01 | 0.00 | 0.02 | 0.01 | 0.01 |
| OH | 1.84 | 2.00 | 1.96 | 0.05 | 1.93 | 2.00 | 2.00 | 0.02 | 2.00 | 2.00 | 2.00 | 0.00 |
| Total (cat) | 8.54 | 8.98 | 8.90 | 0.09 | 8.77 | 9.04 | 8.95 | 0.06 | 8.97 | 9.06 | 9.01 | 0.04 |
| Oct | 1.85 | 2.20 | 2.03 | 0.06 | 1.96 | 2.15 | 2.05 | 0.03 | 2.04 | 2.11 | 2.07 | 0.03 |
| Int | 0.64 | 0.94 | 0.86 | 0.07 | 0.75 | 0.98 | 0.91 | 0.05 | 0.93 | 0.95 | 0.94 | 0.01 |
| Fe + Mg | 0.03 | 0.51 | 0.31 | 0.15 | 0.33 | 0.67 | 0.42 | 0.09 | 0.43 | 0.64 | 0.52 | 0.09 |
| K + Fe + Mg | 0.22 | 1.37 | 1.04 | 0.33 | 1.13 | 1.57 | 1.30 | 0.10 | 1.33 | 1.56 | 1.44 | 0.09 |
| Na/(Na + K) | 0.00 | 0.78 | 0.13 | 0.23 | 0.00 | 0.05 | 0.02 | 0.01 | 0.01 | 0.01 | 0.01 | 0.00 |
| Si/Al | 1.01 | 2.39 | 1.43 | 0.25 | 1.36 | 2.20 | 1.49 | 0.15 | 1.51 | 1.57 | 1.54 | 0.03 |

determine and quantify mineralogy by comparing absorption spectra with a reference library created to fit our case study. The library contains spectra representing different pure minerals and water, as well as selected SWIR spectra of Arroyo Rojo chlorites and white micas with known chemical composition. It covers the wide compositional variations found at the deposit.

## 5. From regional to hydrothermal alteration: mineralogical and geochemical assessment

### 5.1. Regional alteration and metamorphism

The existence of a hydrothermal propylitic association is evident in many samples far from the deposit. This consists of albite, titanite, and clinozoisite, which do not show either a coherent distribution pattern or spatial relation with the VMS-related alteration, which suggests a different origin for that alteration.

Titanite is more abundant in the following members of the study sequence: dacites, ignimbrites, and glassy tuff. It is foliated after regional planar-layered foliation. Titanite chemistry shows Al and Fe content as high as 0.15–0.35 atoms per formula unit (apfu) and >4 wt%, respectively. This agrees with the regional alteration of titanite described in the Abitibi district (Hannington et al., 2003). Clinozoisite has also been described in the district, showing similar $Fe_2O_{3T}$ content (<10 wt%) to that in the Arroyo Rojo deposit. In addition, ferrous chlorites with Fe/(Fe + Mg) values reaching 0.52 have been identified (Biel et al., 2010). According to Hannington et al. (2003), the abundance of ferrous chlorite (Fe/(Fe + Mg) ≥ 0.5), along with titanite and clinozoisite, indicate a regional hydrothermal origin related to fluid circulation associated with a synvolcanic intrusion. This mineral assemblage represents the basal zone of a regional hydrothermal alteration model proximal to a synvolcanic intrusion at $T > 400$ °C (Gifkins et al., 2005).

Albitization and silification are well developed in felsic rocks distal to the mineralized zones; they almost totally replace the original rock (Fig. 3C). This mineral assemblage is typical of the silification zone immediately above the basal zone of the regional hydrothermal alteration model and of fluid temperatures between 300 and 400 °C (Skirrow and Franklin, 1994; Gibson et al., 2000; Gifkins et al., 2005).

According to Caminos (1980), the metamorphic peak reached by the Lemaire rocks is very low, corresponding to the prehnite-pumpellyite facies. The typical mineral assemblage of this facies for submarine volcanic sequences consists of prehnite, pumpellyite and minor chlorite, albite, quartz, epidote, calcite, titanite and, rarely, garnet (see Gifkins et al., 2005 and references therein). The systematic lack of prenhite and pumpellyite in the Arroyo Rojo volcanic sequence is consistent with the regional alteration. These considerations are in accordance with other pervasively altered VMS deposits, such as Mt. Lyell and the Que River (Walshe and Solomon, 1981; Offler and Whitford, 1992), San Telmo, San Miguel and Peña del Hierro from the Iberian Pyrite Belt (IPB) (Sánchez-España et al., 2000) and Noranda (Riverin and Hodgson, 1980), in which low-grade regional metamorphism is only recognizable in zones of dynamic deformation focused along shear zones, such as those occurring in the Arroyo Rojo area.

### 5.2. Hydrothermal alteration

The overlap of metamorphism, deformation, and local mylonitization make the field recognition of alteration zones and lithofacies difficult. However, microscopic, PIMA, and XRD studies allow us to identify different hydrothermal alteration types including silicification, chloritization, sericitization, local albitization, and, more rarely, carbonatization. The main characteristics of the alteration types are the following:

(1) Silicification is a widespread alteration type throughout the volcanic sequence. Its intensity is highly variable and tends to decrease within the massive sulfide zones, where quartz is mainly observed as pressure shadows on pyrite and sphalerite crystals. Under the microscope, silicification occurs as a pervasive development of fine-grained quartz replacing glassy or microcrystalline groundmass of rhyolites and tuffs, embayed quartz and feldspar phenocryst, and phenoclasts, and occasionally occupying intercrystalline spaces. This fine-grained quartz is frequently associated with sericite. In addition, quartz also fills pumice shards and glassy clasts vesicles of tuffs as monocrystals or polycrystalline aggregates (Fig. 3A).
(2) Chloritization is the most pervasive alteration type and is characterized by the development of medium- to fine-grained

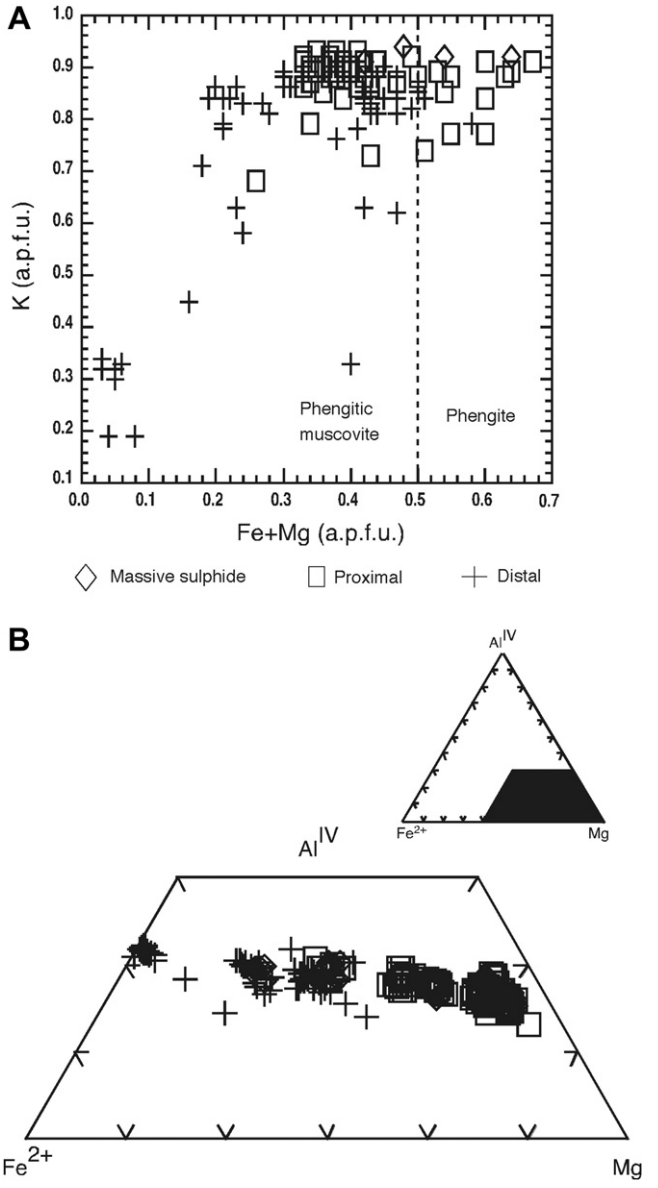


**Fig. 6.** A) K vs. (Fe + Mg) plot showing white mica composition relative to proximity to the massive sulfide lenses; B) $Al^{VI}$–Mg–Fe cation plot showing trend to Mg-rich chlorite with proximity to the massive sulfide lenses.

**Table 2**
Selected electron probe microanalyses of chlorite in the massive sulfide lenses and the related hydrothermal alteration of the Arroyo Rojo deposit (normalized to 28 oxygens $O_{10}(OH)_8$).

| | Distal ($n$ = 100) | | | | Proximal ($n$ = 106) | | | | Massive sulfide ($n$ = 98) | | | |
|---|---|---|---|---|---|---|---|---|---|---|---|---|
| | Min | Max | Med | S.D | Min | Max | Med | S.D | Min | Max | Med | S.D |
| *wt %* | | | | | | | | | | | | |
| $SiO_2$ | 24.01 | 32.76 | 27.55 | 1.99 | 27.30 | 33.21 | 31.10 | 1.65 | 27.74 | 34.87 | 31.00 | 1.44 |
| $TiO_2$ | 0.00 | 0.08 | 0.02 | 0.02 | 0.00 | 0.07 | 0.02 | 0.02 | 0.00 | 1.93 | 0.04 | 0.19 |
| $Al_2O_3$ | 14.15 | 22.63 | 19.66 | 1.43 | 16.06 | 21.43 | 19.14 | 1.22 | 15.77 | 20.40 | 18.60 | 0.93 |
| FeO | 11.30 | 27.08 | 20.50 | 4.83 | 2.36 | 18.98 | 6.49 | 5.54 | 2.35 | 14.46 | 6.57 | 3.22 |
| MnO | 0.00 | 0.58 | 0.20 | 0.19 | 0.17 | 0.65 | 0.37 | 0.13 | 0.14 | 0.64 | 0.41 | 0.09 |
| MgO | 11.04 | 25.96 | 18.54 | 3.73 | 17.36 | 33.05 | 28.95 | 4.44 | 22.03 | 32.73 | 28.77 | 2.28 |
| CaO | 0.00 | 0.75 | 0.07 | 0.10 | 0.00 | 0.18 | 0.06 | 0.05 | 0.00 | 1.48 | 0.06 | 0.15 |
| $Na_2O$ | 0.00 | 0.10 | 0.02 | 0.02 | 0.00 | 0.27 | 0.01 | 0.04 | 0.00 | 0.23 | 0.01 | 0.02 |
| $K_2O$ | 0.00 | 1.87 | 0.15 | 0.36 | 0.00 | 2.26 | 0.10 | 0.35 | 0.00 | 1.16 | 0.09 | 0.19 |
| Total | 95.86 | 102.2 | 98.27 | 1.31 | 96.03 | 102.0 | 98.68 | 1.76 | 95.45 | 100.8 | 97.88 | 1.24 |
| *a.p.f.u.* | | | | | | | | | | | | |
| Si | 2.62 | 3.23 | 2.85 | 0.14 | 2.79 | 3.16 | 3.00 | 0.10 | 2.82 | 3.28 | 3.02 | 0.10 |
| Ti | 0.00 | 0.01 | 0.00 | 0.00 | 0.00 | 0.01 | 0.00 | 0.00 | 0.00 | 0.15 | 0.00 | 0.01 |
| Al IV | 0.77 | 1.38 | 1.15 | 0.14 | 0.84 | 1.21 | 1.00 | 0.10 | 0.72 | 1.18 | 0.98 | 0.10 |
| Al VI | 0.89 | 1.84 | 1.26 | 0.14 | 0.90 | 1.63 | 1.18 | 0.10 | 1.03 | 1.49 | 1.15 | 0.07 |
| Fe | 0.92 | 2.45 | 1.79 | 0.46 | 0.18 | 1.58 | 0.53 | 0.47 | 0.18 | 1.24 | 0.54 | 0.27 |
| Mg | 1.70 | 3.87 | 2.85 | 0.52 | 2.54 | 4.59 | 4.15 | 0.56 | 3.33 | 4.64 | 4.17 | 0.28 |
| Mn | 0.00 | 0.05 | 0.02 | 0.02 | 0.01 | 0.06 | 0.03 | 0.01 | 0.01 | 0.05 | 0.03 | 0.01 |
| Ca | 0.00 | 0.08 | 0.01 | 0.01 | 0.00 | 0.02 | 0.01 | 0.00 | 0.00 | 0.16 | 0.01 | 0.02 |
| Na | 0.00 | 0.02 | 0.00 | 0.00 | 0.00 | 0.05 | 0.00 | 0.01 | 0.00 | 0.04 | 0.00 | 0.00 |
| K | 0.00 | 0.24 | 0.02 | 0.05 | 0.00 | 0.28 | 0.01 | 0.04 | 0.00 | 0.14 | 0.01 | 0.02 |
| Total | 9.57 | 10.07 | 9.95 | 0.08 | 9.75 | 10.04 | 9.92 | 0.05 | 9.68 | 9.99 | 9.92 | 0.05 |
| Oct | 5.36 | 6.06 | 5.90 | 0.12 | 5.44 | 6.00 | 5.86 | 0.08 | 5.48 | 5.94 | 5.86 | 0.07 |
| Int | 0.00 | 0.26 | 0.03 | 0.05 | 0.00 | 0.29 | 0.02 | 0.04 | 0.00 | 0.20 | 0.02 | 0.03 |
| Mg/(Fe + Mg) | 0.48 | 0.78 | 0.61 | 0.10 | 0.66 | 0.96 | 0.88 | 0.10 | 0.74 | 0.96 | 0.89 | 0.06 |
| Fe/(Fe + Mg) | 0.22 | 0.52 | 0.39 | 0.10 | 0.04 | 0.34 | 0.12 | 0.10 | 0.04 | 0.26 | 0.11 | 0.06 |
| Fe + Mg | 3.52 | 5.09 | 4.64 | 0.24 | 3.81 | 5.10 | 4.69 | 0.16 | 3.99 | 4.88 | 4.71 | 0.12 |

and rare radial-growing fan-shaped chlorite as partial or total replacement of tuff matrix and glassy clasts. By contrast, in the massive sulfide lenses chlorite occurs as fine- to coarse-grained aggregates, locally filling cracks. In addition, chlorite occurs as fringes or halos accompanying pressure shadows developed on pyrite and sphalerite crystals in both massive sulfide and disseminated mineralization. As a result, an altered rock composed of more than 90% modal chlorite (chloritite, following Schermerhorn, 1978) is commonly located beneath massive sulfide bodies, especially where country rocks have pyrite-rich stringers (Fig. 3B).

(3) Sericitization is less pervasive than the previously mentioned alteration types in the footwall and more extensive in the hanging wall. Sericitization displays two petrographic types: (1) fine-grained sericite + quartz + (calcite) aggregates partially to totally replacing both K-feldspars phenocrystals and the aphanitic volcanic groundmass, and (2) as elongate coarse-grained aggregates within ore-bodies, forming pressure shadows in relation to disseminated pyrite crystals in the footwall. It is pertinent to our discussion that silicification along with a weak sericitization is the main alteration type in the so-called regional rocks.

(4) Albitization. Although the origins of this process at the Arroyo Rojo deposit still remains controversial, textural evidences suggest two different and overlapped albite formation stages: (a) a regional hydrothermal alteration (e.g., Skirrow and Franklin, 1994; Gibson et al., 2000; Gifkins et al., 2005) characterized by albite fine-grained groundmass replacements of volcanic glass and phenocrysts of the rhyolitic rocks, as well as filling veins (Fig. 3C) and (b) an earlier local hydrothermal alteration, similar to that reported at the IPB by Sánchez-España et al. (2000), evidenced as Na-plagioclase rims and patches replacing primary K-feldspar in weakly altered volcanic rocks.

(5) Carbonatization is rare, but when found, it occurs as spar crystals within sulfides, as filling veinlets and pumice vesicles in the mineralized horizons, and as defining crystal growth zones in quartz, suggesting a late hydrothermal alteration stage

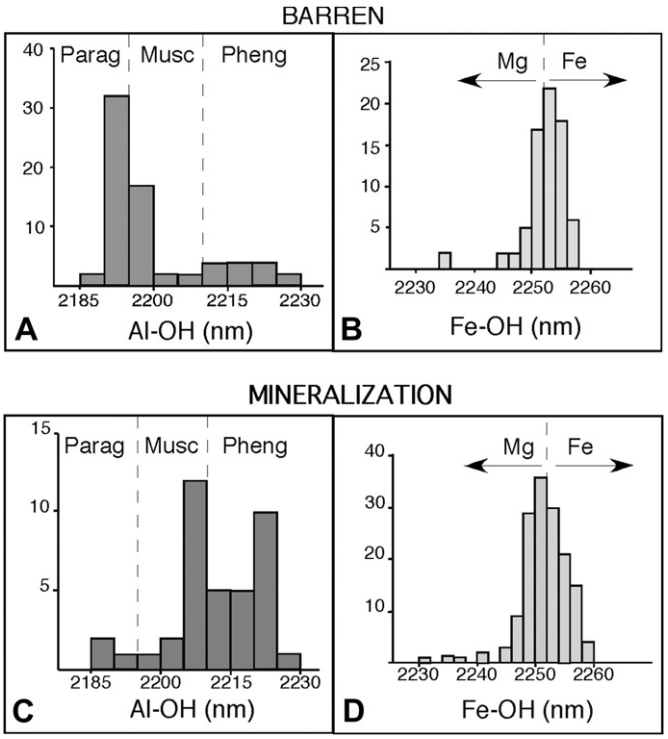


**Fig. 7.** Histograms of white mica Al–OH (A, C) and chlorite Fe–OH (B, D) band wavelengths for barren and mineralized samples.

(Fig. 3D). In the AR6 drill hole (Fig. 2B) calcite appears as fine-grained aggregates commonly associated with micas and lesser amounts of chlorite in the sericitic zones.

The morphology and zonation of the hydrothermal alteration halos associated with the polymetallic Arroyo Rojo deposit fit the stratabound hydrothermal alteration model (Gifkins et al., 2005 and references therein), which is typically parallel to volcanic stratigraphy (Figs. 2B and 4) with a footwall alteration that is more intense and more extensive than the hanging wall alteration. Nevertheless, the mineral replacement of the previously formed seafloor sediments by fluids infilling primary pore spaces in host rocks cannot be disregarded.

From footwall to hanging wall, the mineralogy is as follows (Fig. 4):

*Quartz-Chlorite ± Sericite* is the main footwall alteration assemblage that occurs as a fine-grained groundmass totally replacing volcanic matrix and partially replacing phenocrysts and could be defined as a distal assemblage observed in country rocks away from the mineralized domains. It hosts either barren rocks or disseminated framboidal and euhedral–subhedral aggregates of pyrite crystals, except at the bottom of drill hole AR6, where this alteration assemblage is related to a distinct ore assemblage consisting of semi-massive to massive pyrrhotite showing 120° triple junctions in polygonal grains of granoblastic texture with disseminated framboidal and poliframboidal pyrite and rare chalcopyrite (Fig. 5A). Pressure shadows of quartz, chlorite, and muscovite are also present.

*Quartz-Chlorite*. Passing upward gradually, the chloritization becomes more intense and is associated with disseminated pyrite showing primary depositional textures: framboidal, colloform and euhedral relict cores with concentric growing zonation. Disseminated sphalerite grains display preferred oriented lattice dislocations and develop pressure shadows, primarily of fibrous quartz, in the proximal footwall zone. Quartz veins with subordinate pyrite, sphalerite, and rare chalcopyrite and galena have also been identified as stringers.

*Chlorite±(Quartz-Sericite-Calcite)*. Chloritite is the main hydrothermal alteration product at this level and coexists with massive and semi-massive sulfides, consisting of coarse-grained porphyroblasts of pyrite in a fine-grained and layered matrix of sphalerite with minor chalcopyrite and galena and rare tetrahedrite and bournonite (Fig. 5B). Sphalerite and chalcopyrite display growth twins and deformation textures such as twinning and dislocation lattice, which are also present in pyrite and galena (Fig. 5B and C). Triple junctions in polygonal grains of recrystallized sphalerite, galena, and pyrite are observed. Finally, annealing twins have appeared in sphalerite.

*Quartz-Chlorite ± Calcite*. Deformation and metamorphism are more intense in the proximal hanging wall zone (Fig. 4). Consequently, mylonites, metarhyolites, and brecciated sulfide mineralization are locally present, along with a widespread pyrite and rare disseminated sphalerite mineralization. Pyrite elongation parallel to regional foliation has been observed in mylonites, as well as indentation and sutured grain boundaries. Major pyrite porphyroclasts show aligned cracks and microfractures, which are filled with ductile phases: gangue minerals, sphalerite, chalcopyrite, and galena (Fig. 5D).

*Sericite + Quartz ± Chlorite*. This is the wider hanging wall (Fig. 4) alteration zone, located at the top of the deposit, exhibiting some telescoping with the previously mentioned zone. It occurs as a fine-grained groundmass replacing the volcanic matrix and partially replacing phenocrysts. Although it contains locally disseminated pyrite, it is essentially barren.

## 6. Mineralogical results

### 6.1. X-Ray mineralogy and mineral chemistry

Quartz, feldspars, and phyllosilicates are the most abundant components. Minor amounts of sulfides, mainly pyrite and calcite,

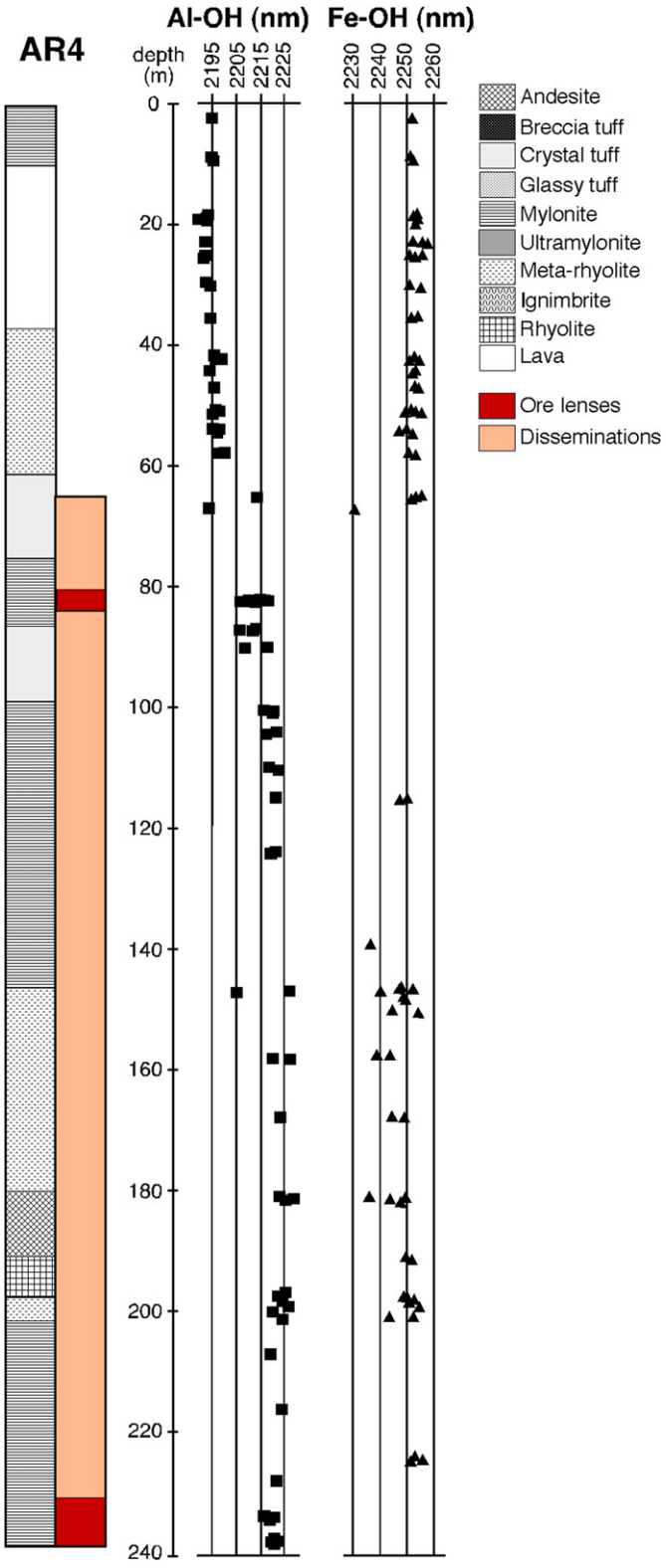


**Fig. 8.** Al–OH band of white mica and Fe–OH band of chlorite of drill hole AR4.

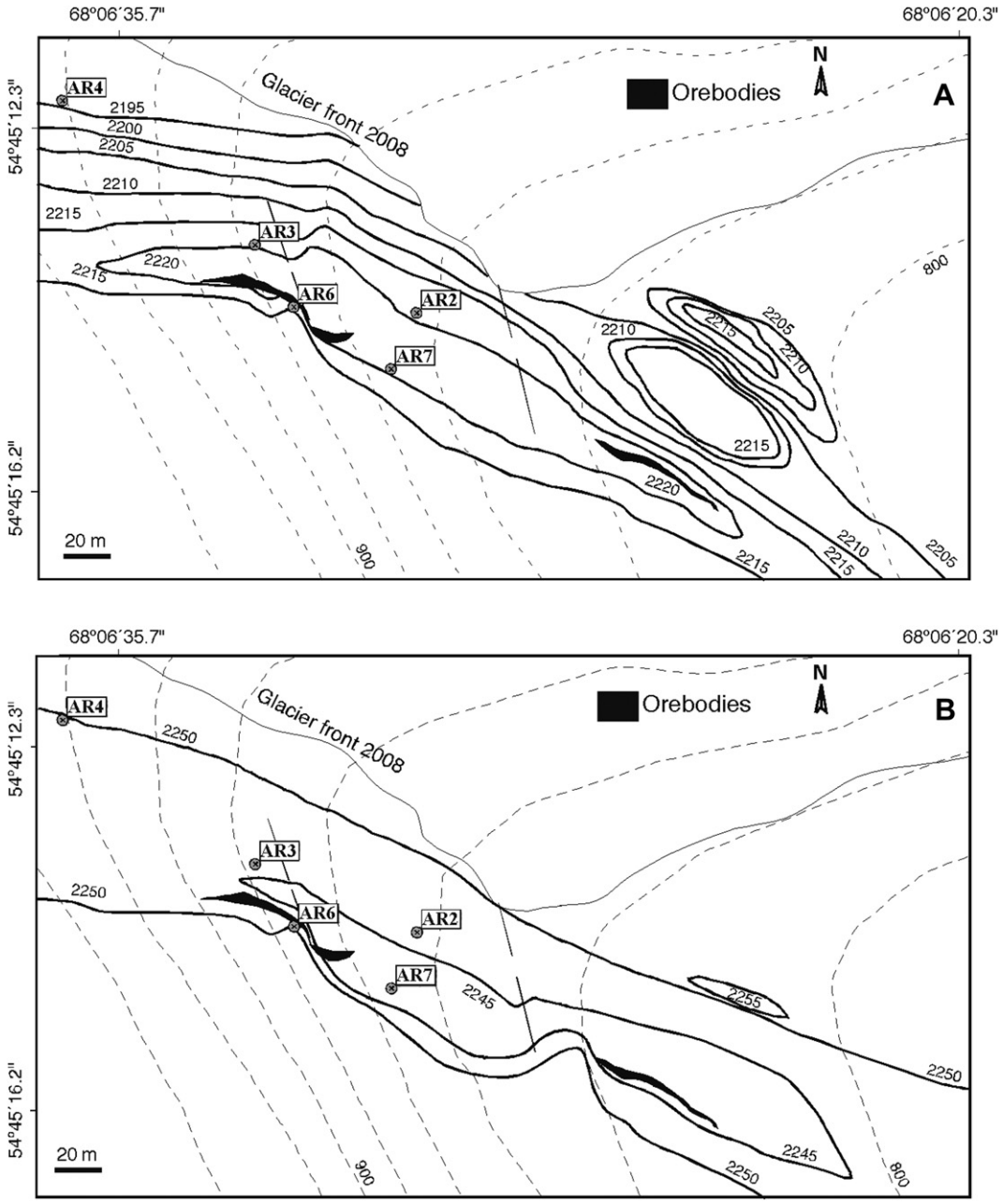


**Fig. 9.** Contour maps of (A) white mica Al–OH band and (B) and chlorite Fe–OH band intensities.

are also present. The phyllosilicates in all lithologies are chlorite and illite.

Electron probe microanalysis (EPMA) shows that chemical composition of white micas (Table 1) is controlled by their spatial position relative to mineralization. Proximal white micas are marked by a more phengitic composition ((Fe + Mg) content and Si/Al ratios) in the proximity of sulfide zones: 0.42 and 1.49, respectively, and 0.52 and 1.54 for ore lenses (Fig. 6A). The immediate outer zones are marked by a less phengitic composition ((Fe + Mg) = 0.31 and Si/Al = 1.43). Paragonite content, expressed by the ratio (Na/(Na + K)), is <0.05 in proximal areas, while in distal areas it is 0.13 (Table 1; Fig. 6A).

Based on EPMA, the chlorites (Table 2, Fig. 6B) close to the sulfide lenses are richer in Mg (4.15 apfu) than distal chlorites, which show Mg content of 2.85 apfu.

### 6.2. Short-wave infrared spectroscopy

The SWIR spectra of white mica associated with mineralization have Al–OH absorption wavelengths ranging from 2189 to 2228 nm with two different populations. The vast majority of the samples vary between 2215 and 2225 nm, and the remainder is set at 2190 nm (Fig. 7). According to Scott et al. (1998), these two populations correspond to phengitic and paragonitic compositions, respectively.

Variations of white mica Al–OH bond absorption wavelengths with lithology show that there is no clear relation between bulk rock composition and white mica spectral features except on rocks lacking white micas, that is, dacite and ignimbrite. In spite of fluctuations in the bulk rock composition, there appears to be a tendency toward increasing Al–OH band wavelength close to

massive sulfide (Fig. 7), highlighting a shift toward more phengitic compositions. In fact, mineralized parts of the sequence show most values between 2205 and 2225 nm (muscovite-phengite), while the non-mineralized parts have values ranging from 2190 to 2200 nm (paragonite). To better demonstrate the relationship between the Al–OH band wavelength and mineralization, an AR4 drill hole is plotted in Fig. 8. The Al–OH band is <2195 nm in its first non-mineralized 40 m and progressively reaches values of >2215 nm in proximity to mineralization. The Al–OH absorption spectral mapping shows increasing Al–OH wavelengths in the proximity of the mineralized lenses, reaching values >2220 nm (Fig. 9A), corresponding with the most important population of mineralized samples (Fig. 7). The Al–OH absorption feature wavelength decreases progressively toward the north, far from the sulfide mineralization and is well observed in the northwest part of the map (Fig. 9A). Fig. 9A demonstrates that spectra distribution is in line with mineralogical distribution because it agrees with the lower white mica content relative to chlorite abundance in proximity to mineralized lenses. This spatial distribution is at odds with the observations at other VMS deposits, such as Myra Falls (Jones et al., 2005) or Western Tharsis (Huston and Kamprad, 2000; Herrmann et al., 2001; Gifkins et al., 2005), in which the Al–OH <2198 band is in the proximity of mineralized zones and progressively increases to values >2204 in distal zones.

This agrees with EPMA data, which show a more phengitic composition in proximity to sulfide zones and less phengitic composition in the immediately outer zones. White mica compositions show a good linear correlation between Al–OH absorption wavelength and phengitic content (Fe + Mg) and Si/Al and (Na/(Na + K)) ratios (Pearson's $r$ of 0.96, 0.81, and −0.86, respectively) (Fig. 10A).

Al–OH wavelength distribution in the Arroyo Rojo deposit shows a sericitic alteration halo of phengitic composition surrounding the main mineralized lenses. The occurrence of phengite in the proximity of ore bodies has been described in other VMS deposits like Prince Lyell (Hendry, 1981), Hellyer (Yang, 1998), Salgandinho (Plimer and Carvalho, 1982), and Draa Sfar (Belkabir et al., 2008).

Variations of chlorite Fe–OH bond absorption wavelength values in the deposit lie between 2231 and 2260 nm, corresponding to Mg in intermediate-Fe chlorite compositions (Pontual et al., 1997; Scott et al., 1998). No mineralized tuffaceous breccias or glass and crystal tuffs show Fe–OH wavelengths absorption values ranging from 2230 to 2260 nm (Fig. 7). The lower values in this range (<2250 nm) correspond to Fe/(Fe + Mg) values from 0.04 to 0.26 for proximal samples, whereas values >2250 correspond to Fe/(Fe + Mg) from 0.26 to 0.36 for distal samples, showing a general decreasing of Fe–OH wavelength as the proximity to massive sulfides increases (Fig. 9B). Although this tendency is graphically depicted in Fig. 7, showing that the majority of wavelength values are <2252 nm for mineralized areas and those >2252 nm for non-mineralized areas, it is better defined in the AR4 drill hole (Fig. 8). In this drill hole, Fe–OH absorption wavelength decreases sharply in mineralized zones.

The Fe–OH absorption spectral mapping shows ≤2245 nm values in the proximity of the mineralized lenses, reaching >2250 nm values in distal zones. This increase is more evident at the top of the deposit, as is observable in the SW part of the map (Fig. 9B). This tendency is similar to that of the Myra Falls deposit (Jones et al., 2005), where chlorite Fe–OH wavelength decreases progressively from >2250 nm to <2240 nm values in mineralized zones.

As with the white mica, a comparison of spectral data with chlorite compositions yields very good results. There is a linear correlation of $r = -0.74$ between the chlorite Mg number (100Mg/(Mg + Fe)) and the Fe–OH absorption feature (Fig. 10B). Consequently, the highest Mg/(Mg + Fe) values, varying between 0.66 and 0.96, correspond to the proximal zone, while values ranging between 0.48 and 0.78 are those from the distal areas. This contrasts noticeably with previous studies (Herrmann et al., 2001; Jones et al., 2005) in which Fe–OH absorption feature has no significant correlation to chlorite composition.

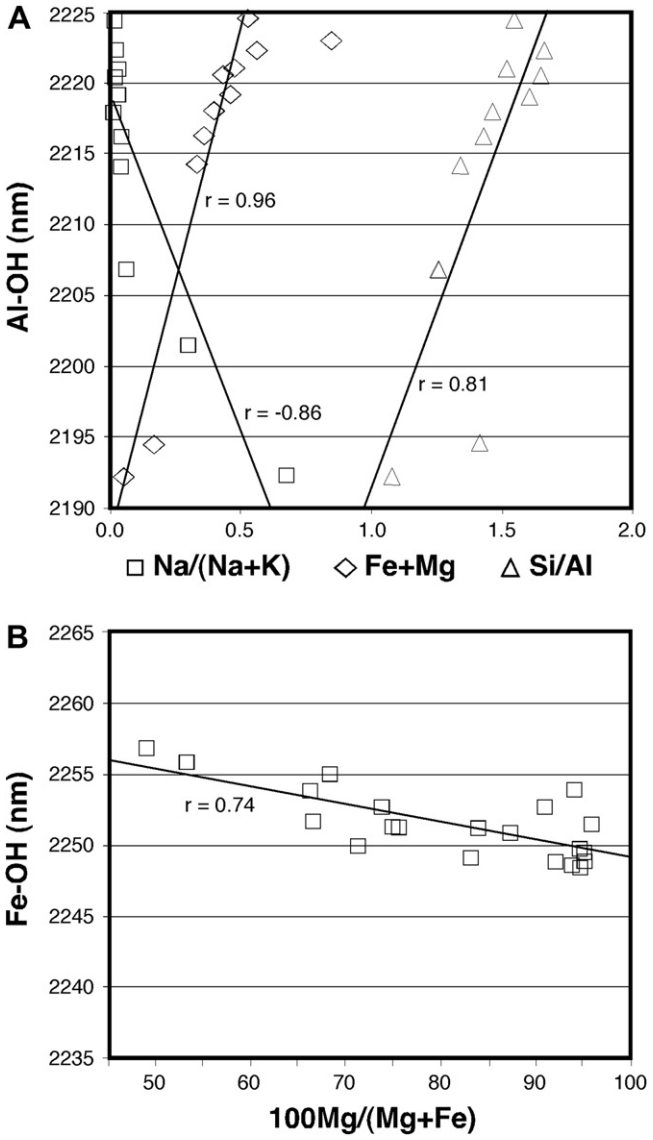


**Fig. 10.** PIMA data vs. EPMA chemical data for (A) white micas and (B) chlorites from the Arroyo Rojo prospect. $r$: Pearson product correlation coefficient; Mg#: 100Mg/(Mg + Fe).

According to McLeod and Stanton (1984), this distribution indicates a chlorite alteration pattern with an inner Mg-chlorite core and an intermediate to ferrous chlorite external zone. This pattern has also been observed in other VMS deposits, such as Thalanga (Paulick et al., 2001), Noranda (Riverin and Hodgson, 1980), Myra Falls (Jones et al., 2005) and at the Japanese Kuroko deposits (Urabe et al., 1983).

Regional rock samples taken from Lemaire Formation outcrops far from the mineralization have also been analyzed with infrared techniques for comparison purposes (Fig. 11). Weak silicification and sericitization and rare chloritization are the main alteration types of the regional rocks. The obtained chlorite spectra show Fe–OH band ranges between 2240 and 2259 nm, with most of the

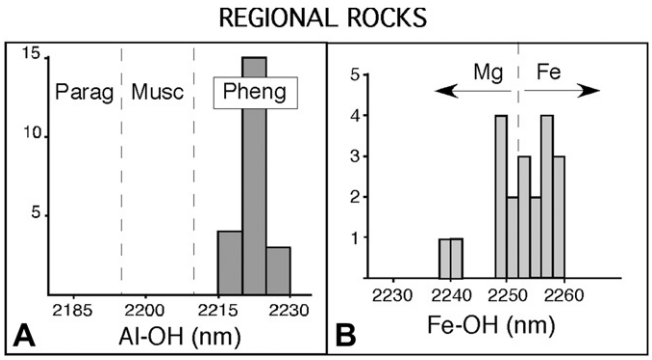


**Fig. 11.** Histograms of (A) white mica Al–OH and (B) chlorite Fe–OH band wavelengths for regional rocks.

values between 2250 and 2258 nm, matching those from distal areas at the Arroyo Rojo deposit. Therefore, ferrous chlorite may be the result of regional hydrothermal alteration or metamorphism. White mica Al–OH absorption features do not fit as well with the Arroyo Rojo trends as the chlorite spectra. Values varying from 2216 to 2229 nm are higher than those from the distal zone at the Arroyo Rojo deposit (Fig. 7). This result may be due to a local distribution pattern of white mica alteration in the deposit caused by hydrothermal alteration overprinting over regional alteration, metamorphic or diagenetic weathering. An external paragonitic zone surrounding the main sericitic zone has also been described in the VMS deposits of Aljustrel and Neves Corvo (Relvas et al., 1997), both of which display a stratabound hydrothermal alteration model similar to that of Arroyo Rojo.

## 7. Conclusions

(1) At Arroyo Rojo, massive sulfide lenses are developed at several levels and are connected by a zone of stringers or alterations with disseminated sulfides. Hydrothermal alteration, regional metamorphism (greenschist facies), and local mylonitization have modified the Arroyo Rojo stratigraphic sequence.

(2) The strongest hydrothermal alteration occurs immediately below the ore lenses. This alteration consists of the assemblage chlorite ± quartz ± sericite ± calcite. Zones of strong sericitization are present elsewhere. Silicified zones occur primarily as stringers, and albitized and carbonatized zones occur only locally.

(3) Chlorite and mica compositions show systematic trends relative to spatial distribution: from Mg-rich chlorite and phengite-phengitic muscovite in proximal zones to Fe-rich chlorite and paragonitic muscovite in distal areas.

(4) Chlorite and white mica SWIR-characteristic bands have been used to delimit the mineralized lenses and to define subzones within the chlorite and sericite zones. The Al–OH and Fe–OH absorption wavelengths can be considered diagnostic of mineralization: 2220 nm and 2252 nm for white mica and chlorite, respectively, define a sharp zone enveloping the massive sulfide mineralization. Both Al–OH and Fe–OH absorption features have a significant correlation with white mica and chlorite compositions. Different lithologies generally show a similar range of Al–OH and Fe–OH absorption features, suggesting that lithology did not play a major role in determining the degree of alteration.

(5) The combination of mineralogical and spectral techniques confirms the applicability of PIMA as an effective exploration and vectoring tool in areas like Tierra del Fuego.

## Acknowledgments

We gratefully acknowledge the Dirección General de Recursos Mineros of the Tierra del Fuego province for providing access to drill cores. This study was funded by the Spanish Ministerio de Ciencia e Innovación Project CGL2007-61095. The Grupo de Recursos Minerales is supported by the Gobierno de Aragón. The Spanish Ministerio de Educación y Ciencia financially supports Cecilia Biel (grant FPU scheme) (AP2005-0244). We are grateful to Dave Lentz and Patrick Mercier-Langevin for their helpful comments, which improved this manuscript.

## References

Ametrano, S., Etcheverry, R., Echeveste, H., Godeas, M., Zubia, M., 2000. VMS district of Tierra del Fuego, Argentina. In: Sherlock, R., Logan, M.A.V. (Eds.), VMS Deposits of Latin America. Special Paper. Geological Association of Canada, pp. 593–612.

Barker, P.F., 2001. Scotia Sea regional tectonic evolution: implications for mantle flow and palaeocirculation. Earth-Science Reviews 55, 1–39.

Belkabir, A., Gibson, H.L., Marcoux, E., Lentz, D., Rziki, S., 2008. Geology and wall rock alteration at the Hercynian Draa Sfar Zn-Pb-Cu massive sulphide deposit, Morocco. Ore Geology Reviews 33, 280–306.

Biel, C., Subías, I., Fanlo, I., Acevedo, R.D., 2007. Mineralogical Characterization of Lemaire and Yahgán Formations, Tierra del Fuego, Argentina. GeoSur 23.

Biel, C., Subías, I., Fanlo, E., Mateo, E., Acevedo, R.D., 2010. The Arroyo Rojo volcanic-hosted massive sulphide deposit (Tierra del Fuego, southernmost Argentina): geology, mineralogy, petrography and mineral chemistry. Revista Mexicana de Ciencias Geológicas 27, 84–96.

Broili, C., Klohn, M., Hodder, R.W., 2000. Exploration, geology and mineral deposits in the Fin del Mundo project, Tierra del Fuego, Argentina. In: Sherlock, R., Logan, M.A.V. (Eds.), VMS Deposits of Latin America. Special Paper. Geological Association of Canada, pp. 567–591.

Caminos, R., 1980. Cordillera Fueguina, Geología Regional Argentina. Academia Nacional de Ciencias, Córdoba, pp. 1463–1501.

Dalziel, I.W.D., Dewit, M.J., Palmer, K.F., 1974. Fossil Marginal basin in southern Andes. Nature 250, 291–294.

Gibson, H.L., Santaguida, F., Paquette-Mihalasky, F.I., Watkinson, D.H., 2000. Evolution of regional semiconformable alteration assemblages within an Archean subseafloor hydrothermal system, and relationship to VMS deposits, at Noranda, Quebec, Canada. In: Gemell, J.B., Pongratz, J. (Eds.), Volcanic Environments and Massive Sulphide Deposits. CODES (Centre for Ore Deposit Research) Special Publication, vol. 3, pp. 61–63.

Gifkins, C., Hermann, W., Large, R., 2005. Altered Volcanic Rocks. A Guide to Description and Interpretation. CODES (Centre for Ore Deposit Research), Tasmania, 288 pp.

Hannington, M.D., Santaguida, F., Kjarsgaard, I.M., Cathles, L.M., 2003. Regional-scale hydrothermal alteration in the Central Blake River Group, western Abitibi subprovince, Canada: implications for VMS prospectivity. Mineralium Deposita 38, 393–422.

Hendry, D.A.F., 1981. Chlorites, phengites and siderites from the Prince Lyell ore deposit, Tasmania, and the origin of the deposit. Economic Geology 76, 285–303.

Herrmann, W., Blake, M., Doyle, M., Huston, D., Kamprad, J., Merry, N., Pontual, S., 2001. Short wavelength infrared (SWIR) spectral analysis of hydrothermal alteration zones associated with base metal sulfide deposits at Rosebery and Western Tharsis, Tasmania, and Highway-Reward, Queensland. Economic Geology 96, 939–955.

Huston, D.L., Kamprad, J., 2000. The Western Tharsis deposit. A "high sulphidation" Cu-Au deposit in the Mt Lyell field, of possible Ordovician age. AGSO Research Newsletter 32, 2–6.

Jones, S., Herrmann, W., Gemmell, J.B., 2005. Short wavelength infrared spectral characteristics of the HW horizon: implications for exploration in the Myra Falls volcanic-hosted massive sulfide Camp, Vancouver island, British Columbia, Canada. Economic Geology 100, 273–294.

McLeod, R.L., Stanton, R.L., 1984. Phyllosilicates and associated minerals in some Paleozoic stratiform sulfide deposits of southeastern Australia. Economic Geology 79, 1–21.

Martin, J.D., 2004. Using XPowder: A Software Package for Powder X-Ray Diffraction Analysis. www.xpowder.com D.L. GR 1001/04. ISBN: 84-609-1497-6, Spain.

Offler, R., Whitford, D.J., 1992. Wall rock alteration and metamorphism of a volcanogenic massive sulfide deposit at Que River, Tasmania: petrology and mineralogy. Economic Geology 87, 686–705.

Olivero, E.B., Martinioni, D.R., 2001. A review of the geology of the Argentinian Fuegian Andes. Journal of South American Earth Sciences 14, 175–188.

Paulick, H., Herrmann, W., Gemmel, J.B., 2001. Alteration of felsic volcanics hosting the Thalanga massive sulfide deposit (Northern Queensland, Australia) and geochemical proximity indicators to ore. Economic Geology 96, 1175–1200.

Plimer, I.R., Carvalho, D., 1982. The geochemistry of hydrothermal alteration at the Salgadinho copper deposit, Portugal. Mineralium Deposita 17, 193–211.

Pontual, S., Merry, N., Gamson, P., 1997. G-Mex Volume 1. Spectral Interpretation Field Manual. Ausspec International Pty. Ltd., Kew, Victoria 3101, Australia, 169 pp.

Relvas, J.M.R.S., Barriga, F.J.A.S., Ferreira, A., Noiva, P.C., Carvalho, P., 1997. Footwall alteration and stringer ores, Corvo orebody, Neves. Corvo, Portugal. In: Barriga, F.J.S. (Ed.), SEG Neves Corvo Field Conference, p. 93.

Riverin, G., Hodgson, C.J., 1980. Wall-rock alteration at the Millenbach Cu-Zn mine, Noranda, Quebec. Economic Geology 75, 424–444.

Sánchez-España, J., Velasco, F., Yusta, I., 2000. Hydrothermal alteration of felsic volcanic rocks associated with massive sulphide deposition in the northern Iberian Pyrite Belt (SW Spain). Applied Geochemistry 15, 1265–1290.

Schermerhorn, L.J.G., 1978. Epigenetic magnesiam metasomatism or syngenetic chloritite metamorphism at Falun and Orijärvi. Institution of mining and Metallurgy Transactions, Section B Applied Earth Science 87, 162–167.

Scott, K.M., Yang, K., Huntington, J.F., 1998. The Application of Spectral Reflectance Studies Chlorites in Exploration, CSIRO EM Report 545R, pp. 1–43.

Skirrow, R.G., Franklin, J.M., 1994. Silicification and metal leaching in subconcordant alteration zones beneath the Chisel Lake massive sulphide deposit, Snow Lake, Manitoba. Economic Geology 89, 31–50.

Urabe, T., Scott, S.D., Hattori, K., 1983. A comparison on footwall-rock alteration and geothermal systems beneath some Japanese and Canadian volcanogenic massive sulphide deposits. Economic Geology Monograph 5, 345–364.

Walshe, J.L., Solomon, M., 1981. An investigation into the environment of formation of the volcanic-hosted Mt. Lyell cop- per deposits using geology, mineralogy, stable isotopes, and a six-component chlorite solid solution model. Economic Geology 76, 246–284.

Yang, K., 1998. Compositional Variation of White Micas. A Literature Review. CSIRO, North Ryde, pp. 1–23.